PHYSICAL REVIEW D **78,** 075026 (2008)

Describing viable technicolor scenarios

Johannes Hirn[*] and Adam Martin[+]
Department of Physics, Yale University, New Haven, Connecticut 06520, USA

Verónica Sanz[‡]
Department of Physics, Boston University, Boston, Massachusetts 02215
and Department of Physics and Astronomy, York University, 4700 Keele Street, Toronto, Ontario M3J 1P3
(Received 25 July 2008; published 24 October 2008)

We construct an effective Lagrangian for new strong interactions at the LHC, including as a first step the two lightest triplets of spin-1 resonances. Our parametrization is general enough to allow for previously unstudied spectrum and couplings. Among available frameworks to describe the spin-1 sector, we rely on an extra-dimensional description. Our approach limits the number of parameters yet is versatile enough to describe the phenomenology of a wide range of new scenarios of strong electroweak symmetry breaking.

DOI: 10.1103/PhysRevD.78.075026 PACS numbers: 12.60.Nz, 12.60.Rc

I. INTRODUCTION

The approach of LHC turn-on has renewed interest in dynamical electroweak symmetry breaking (DEWSB), whether in the traditional form of Technicolor models [1–3], or that of its possible 5D dual description [4,5] and related moose models [6,7]. Yet, only a handful of nonsupersymmetric models of electroweak symmetry breaking have so far been implemented in Monte Carlo generators [8–10].

To pave the way for more simulations of DEWSB, we define a flexible framework with resonances and more generic interactions than have previously been considered. At the same time, we strive to limit the number of parameters in this Lagrangian, to make the parameter space manageable. Dialing the parameters then allows one to describe a sampling of strong interaction models, as mSUGRA did for the MSSM: our framework is intended to work in a similar way, applied to DEWSB. We have already presented some phenomenological applications in [11]; the present paper details the inner workings of our framework.

In practice, our approach extends attempts to model strong interactions, based on the ideas of hidden local symmetry [12–15] and mooses [16,17] as well as 5D warped models [18,19] (themselves inspired by AdS/CFT [20–22]). These approaches have been used for QCD [23–26] with some accuracy, and thus tend to describe strong interactions which closely follow QCD behavior up to a rescaling of N_c and Λ_{QCD}. For instance, they all predict the following: (1) the spectrum consists of an alternance of states with definite parity, implying that only half of the neutral resonances couple to WW scattering, (2) the lightest resonance has vector parity, and (3) the photon couplings to two different particles vanish (the equivalent of $a_1 \to \pi\gamma$ vanishing in QCD [27]).

To explore different scenarios, we will build on a previous construction—Holographic Technicolor (HTC) [28]—in which the new strong interactions can differ from rescaled QCD. In addition to their allowing new phenomena, deviations from QCD may help alleviate difficulties with electroweak precision tests [29]. HTC uses 5D language but, compared to Higgsless models [30], it adds deviations from pure AdS 5D geometry in the form of effective warp factors which differ for the various fields. As the name *effective warp factors* implies, we are only borrowing 5D language to describe a 4D scenario. Therefore, it does not matter that simple 5D models do not reproduce these effective warp factors by using bulk scalars [31]. Indeed, the same physics could be obtained in a purely 4D context by using moose notation [32].

In the present paper, we use the HTC language to model the resonances and SM gauge boson sectors. The main constraint on such interactions comes from experimental bounds on trilinear gauge couplings (TGCs). However, a phenomenological study also requires modeling the fermion-resonance interactions. In the present phenomenological description, these couplings are simply assigned by hand: we fix the couplings between fermions and resonances to pass current limits. (Modelling the fermions in 5D would unnecessarily increase the number of parameters in our study. On the other hand, it may bring interesting consequences, such as a preferential coupling of the resonances to third generation fermions.) The present paper deals with the low-energy Lagrangian and its relation with the 5D description. Phenomenological studies for a few benchmark points were presented previously [11].

We start in Sec. II by describing the interactions in an effective Lagrangian of spin-1 resonances. In Sec. III, we then discuss our HTC framework for reducing the number of parameters as compared to a generic effective

[*]johannes.hirn@yale.edu
[+]adam.martin@yale.edu
[‡]vsanz@bu.edu

 © 2008 The American Physical Society

Lagrangian, and its relation to 5D modelling. In Sec. IV, we detail some important properties of the model relative to the parity of resonances. In Sec. V, we study the constraints that TGC bounds from LEP impose on the parameter space of HTC. Section VI explores the predictions of the model for two interesting regions of parameter space.

II. EFFECTIVE LAGRANGIAN: CUBIC INTERACTIONS

We consider a spectrum consisting of the SM spin-1 fields (γ, W, Z), two triplets of resonances, as well as the SM quarks and leptons, but no physical Higgs particle. We refer to the resonances as $(W_{1,2}^{\pm}, Z_{1,2})$ rather than $(\rho_T^{\pm,0}, a_1^{\pm,0})$ since they will turn out to lack a definite parity, see Sec. IV.

In this section, we detail the cubic couplings of dimension 4 between spin-1 fields. We restrict ourselves to cubic vertices involving one resonance and quartic vertices with SM fields, as is sufficient to study the production of new heavy states at the LHC. Even at this level, we need to make assumptions to limit the independent parameters to a manageable number. We will use HTC to this effect in Sec. III.

A. Deviations from SM couplings

The presence of a new sector affects the self-couplings of SM gauge fields, introducing deviations from the SM in the TGCs. In this paper, we will consider constraints from the following TGCs [33]:

$$\begin{aligned}\mathcal{L} \supset & -ie((\partial_{[\mu}W^-_{\nu]}W^{+\mu}A^{\nu} + \partial_{[\mu}W^+_{\nu]}A^{\mu}W^{-\nu}) \\ & + \kappa_\gamma \partial_{[\mu}A_{\nu]}W^{-\mu}W^{+\nu}) - ie\frac{c}{s}(g_1^Z(\partial_{[\mu}W^-_{\nu]}W^{+\mu}Z^{\nu} \\ & + \partial_{[\mu}W^+_{\nu]}Z^{\mu}W^{-\nu}) + \kappa_Z \partial_{[\mu}Z_{\nu]}W^{-\mu}W^{+\nu}),\end{aligned} \tag{1}$$

where κ_γ, g_1^Z, κ_Z can differ from their SM value (equal to 1). c and s in Eq. (1) are the cosinus and sinus of the Weinberg angle.

From (1) above, we see that the $WW\gamma$ interaction is in general built up of two separate Lorentz structures with independent couplings (e and $e\kappa_\gamma$). The WWZ interactions also contains two independent couplings (g_1^Z and κ_Z). Most scenarios of DEWSB impose $\kappa_\gamma = 1$ and $\kappa_Z = g_1^Z$ (see Sec. VI C). Current bounds on the TGCs (1) will restrict the parameters in our description of strong interactions (Sec. V).

B. Resonance couplings

Introducing the spin-1 resonances as massive gauge fields generically called B^-, C^+, D^0, we consider the following dimension-4 cubic couplings

$$\begin{aligned}\mathcal{L} \supset & -i(g_{BCD1}\partial_{[\mu}B^-_{\nu]}C^{+\mu}D^{0\nu} + g_{BCD2}\partial_{[\mu}C^+_{\nu]}D^{0\mu}B^{-\nu} \\ & + g_{BCD3}\partial_{[\mu}D^0_{\nu]}B^{-\mu}C^{+\nu}),\end{aligned} \tag{2}$$

where the three independent couplings $g_{BCD1} \neq g_{BCD2} \neq g_{BCD3}$ are consistent with all the low-energy symmetries. The number of free couplings thus increases quickly as we include more resonances: we find 45 new couplings if we limit ourselves to the $W^{\pm}$, Z and two triplets of resonances.

Specializing to photon couplings, i.e. $D = \gamma$, the unbroken $\mathrm{U}(1)_{\mathrm{em}}$ gauge invariance imposes on (2) the following relation:

$$g_{BC\gamma} = 0, \quad \text{if } B \neq C, \tag{3}$$

while there is no constraint on the third coupling in (2)

$$g_{BC\gamma 3} \neq 0, \quad \text{if } B \neq C. \tag{4}$$

This yields seven cubic couplings involving the photon. The presence of a coupling between the photon and two different particles of unequal masses, explored recently [10,34], produces striking signals in collider studies [11].

Although we have restricted ourselves to cubic vertices, the number of parameters is already $\mathcal{O}(50)$, far too large for a collider study. Section III will introduce Holographic Technicolor (HTC) [28], the framework we use to reduce the number of parameters.

C. Fermion couplings

In this paper we *define* the interactions of the fermions by setting their couplings to the W, Z mass eigenstates by hand to obey the SM relations.

Usually, S and T are defined from two-point functions of W and Z, or from operators in an effective Lagrangian like W^3B. Here we follow a different procedure by working directly in the mass basis where there are no mixing operators which would contribute to the S and T parameters. Moreover, by imposing SM couplings between fermions and W, Z and γ, we ensure that the amplitudes extracted experimentally satisfy $S = T = 0$. This can be read off from the expression for the neutral current amplitude [35]

$$\begin{aligned}\mathcal{M}_{\mathrm{NC}} = & e^2\frac{\mathcal{Q}\mathcal{Q}'}{Q^2} + \frac{(I_3 - s^2\mathcal{Q})(I_3' - s^2\mathcal{Q}')}{\frac{1}{4\sqrt{2}G_F} - s^2c^2M_Z^2\frac{T}{4\pi} + (\frac{s^2c^2}{e^2} - \frac{S}{16\pi})Q^2} \\ & + \text{non-oblique contributions.}\end{aligned} \tag{5}$$

Our phenomenological study is not intended to present a UV completion that would resolve the clashes between DEWSB and oblique corrections. Rather, it tries to present the possible phenomenological consequences of a scenario that would pass the oblique and TGC constraints (Sec. V).

We set the couplings of fermions to the resonances to be compatible with experimental bounds from LEP and Tevatron [36–42].

III. 5D WITH A TWIST

To keep the study manageable in the spin-1 sector, we use 5D techniques, trading the plethora of resonance couplings in (2) for a few extra-dimensional parameters.

The usual reason for using 5D models to describe 4D strongly interacting theories is the AdS/CFT correspondence [20–22]. Although rigorous derivations of this duality have only been obtained for very specific cases, we do not need an exact equivalence in order to study LHC phenomenology. Indeed, provided the essential properties of the 5D model are the same as the strong interaction scenario, we can use the 5D description as a physical guide and organizing scheme. The 5D description also allows for the introduction of deviations from rescaled QCD, using for instance Holographic Technicolor (Sec. III B).

A. 5D Basics

We quickly review the extra-dimensional properties and language we need. The geometry of the extra dimension is described by the warp factor $w(z)$, as in the line element

$$ds^2 = w(z)^2(\eta_{\mu\nu}dx^\mu dx^\nu - dz^2). \tag{6}$$

The z-coordinate is finite, extending from l_0 (UV brane) to l_1 (IR brane). A gauge field propagating in the 5D spacetime, $A_M(x^\mu, z)$ possesses five indices $M = (\mu, 5)$, and can be decomposed as an infinite sum of 4D excitations

$$A_M(x, z) = \sum_n^\infty a_M^{(n)}(x^\mu)\varphi_M^{(n)}(z). \tag{7}$$

$\varphi_M^{(n)}(z)$ is the wave function, or profile, of the 4D field $a_M^{(n)}(x)$ along the extra dimension z (in the *bulk*). This Fourier decomposition is called in this context *Kaluza-Klein* (KK) decomposition, and the infinite tower of KK excitations, the KK tower.

The wave functions $\varphi_M^{(n)}(z)$ are obtained by solving the equation of motion of the field A_M in the background given by $w(z)$. The wave functions also depend on the boundary conditions (BCs) imposed at l_0 and l_1. One can choose BCs to partly or completely break the 5D gauge symmetries at low energies. Specifically, if the BCs do not allow massless (i.e. flat) modes in the spectrum, then there is no remaining 4D gauge invariance.

Once the wave functions are known, the interactions between 4D fields can be derived from overlap integrals. For example, the coupling of the Z and W bosons to a resonance W_i is the integral of their wave functions along the z-coordinate,

$$g_{ZW\rho} \propto \int_{l_0}^{l_1} \frac{dz}{g_5^2} w(z)\varphi_Z\varphi_W\varphi_{W_i}\ldots. \tag{8}$$

Such couplings can be computed easily, yielding from the Lagrangian (9) the value of all the cubic couplings of SM gauge fields (1) and resonances (2).

For a given choice of gauge group, BCs and geometry, a 5D model uses only a few parameters to describe a complex scenario of many particles. In the simplest version (AdS), these parameters are the length l_1, the dimensionless gauge coupling l_0/g_5^2, and the form of the geometry $w(z) = \frac{l_0}{z}$. In the following we introduce *two* more parameters in the functional shape of the warp factors. These two new parameters are an essential ingredient to achieve a departure from QCD-like physics (Sec. III C) while maintaining 5D relations such as (8).

B. The Lagrangian of Holographic Technicolor

To model DEWSB, we place $SU(2)_L \otimes SU(2)_R$ gauge fields in the 5D bulk. The lightest KK excitations of these 5D gauge fields correspond to the SM elecroweak gauge bosons, while the higher KK excitations of the same 5D fields will be interpreted as resonances. HTC corresponds to the following choice of bulk action:

$$S = -\frac{1}{4g_5^2}\int d^4xdz \frac{w_V(z) + w_A(z)}{2}(F^a_{L,MN}F_L^{a,MN} + F^a_{R,MN}F_R^{a,MN}) + (w_V(z) - w_A(z))F^a_{L,MN}F_R^{a,MN}, \tag{9}$$

where a labels the SU(2) generator. We chose to write a bulk Lagrangian invariant under $L \leftrightarrow R$, i.e. parity. In that case, it is convenient to work in terms of the vector and axial combinations of gauge fields $V, A = (R \pm L)/\sqrt{2}$, to get

$$S = -\frac{1}{4g_5^2}\int d^4xdz(w_V(z)F^a_{V,MN}F_V^{a,MN} + \omega_A(z)F^a_{A,MN}F_A^{a,MN}),$$

where

$$F_{V,MN} = \partial_M V_N - \partial_N V_M - \frac{i}{\sqrt{2}}([V_M, V_N] + [A_M, A_N]), \tag{10}$$

$$F_{A,MN} = \partial_M A_N - \partial_N A_M - \frac{i}{\sqrt{2}}([V_M, A_N] + [A_M, V_N]). \tag{11}$$

We use Higgsless BCs in the IR

$$A^a|_{\mathrm{IR}} = 0, \qquad \partial_z V^a|_{\mathrm{IR}} = 0. \tag{12}$$

The UV BCs appropriate for EWSB break parity, which will have consequences later on (Sec. IV)

$$\partial_z(V^a - A^a)|_{\mathrm{UV}} = 0, \tag{13}$$

$$V^{1,2} + A^{1,2}|_{\mathrm{UV}} = 0, \tag{14}$$

$$\Delta\partial_z(V^3 + A^3)|_{\mathrm{UV}} = g_5^2\Box_4(V^3 + A^3)|_{\mathrm{UV}}. \tag{15}$$

The third BC in (15) is achieved by adding a brane-localized U(1) kinetic term [43]

$$-\frac{1}{4\Delta}(\partial_{[\mu}R^3_{\nu]}\partial^{[\mu}R^{\nu]3}), \tag{16}$$

and requiring that the variation of the action vanish under any variation of R^3_μ. This allows for a $U(1)_{B-L}$ brane field.[1]

The above combination of BCs ensures that the only surviving symmetry at low energies is $U(1)_{\rm em}$. Other than the photon massless mode, the spectrum contains the massive Z and $W^\pm$ and an infinite tower of heavier resonances $(W^\pm_i, Z_i)$. For given warp factors $w_A(z)$, $w_V(z)$, l_1 sets the mass of the lightest resonance in the KK tower with respect to M_W. We will be interested in cases where the lightest resonance is lighter than 1 TeV, and we will truncate the KK tower after the lightest two triplets. One consequence of adding a sizeable $F_L F_R$ term in (9) is that the two first triplets can have comparable masses, and therefore must both be kept in the spectrum.

C. Breaking patterns

As mentioned above, 5D models in AdS, in which there is only one warp factor with a fixed expression $w_A(z) = w_V(z) = \frac{l_0}{z}$, exhibit features similar to a rescaled version of QCD (alternating spectrum with selection rules for couplings). Allowing two different warp factors which deviate from AdS in the infrared, as in HTC (9), lifts these restrictions.

For computations, we need to pick an explicit expression form for the warp factors: we choose the positive-definite

$$w_{A,V}(z) = \frac{l_0}{z} e^{o_{A,V}/2(z-l_0/l_1)^4}. \tag{17}$$

We use the name *effective warp factors* because $w_{A,V}$ do not correspond to an actual geometry in 5D [31]. Rather, $w_{A,V}$ parameterize different scenarios of technivectors: varying $o_{V,A}$ amounts to changing the masses and couplings of the vector and axial resonances. The exact power of z in (17) is not crucial: a modification of the power could be partly absorbed in a modification of o_V, o_A. What matters is that the effective metrics deviate from AdS in the IR, and thus modify the wave functions and overlap integrals (8) from which the couplings are obtained.

Beyond the breaking by IR BCs, familiar from Higgsless theories [44]), the different effective metrics felt by the V and A fields introduce symmetry breaking in the bulk (z-dependence). Brane-breaking corresponds to the choice of BCs in (12), while bulk-breaking is introduced on top of (12) as different effective metrics in (9)

$$\text{brane-breaking} \Rightarrow w_A(z) = w_V(z),$$
$$\text{bulk-breaking} \Rightarrow w_A(z) \neq w_V(z).$$

In the case of brane-breaking, the only distinction between the broken (axial) and unbroken (vector) generators comes from the IR BCs. In a "dual" interpretation, where the fifth space coordinate is inversely related with an energy scale, this corresponds to the symmetry breaking occurring suddenly at the resonance scale [5]. The localization of the breaking at a point in the extra dimension suppresses effects at any scale above that. Such hard-wall breaking is the crudest 5D model of spontaneous symmetry breaking.

If the symmetry breaking is turned on progressively along the 5th dimension rather than at the IR brane alone, we have bulk-breaking. The strength of the breaking, and therefore the difference between the properties of vector and axial states, is governed by the z-dependence of the breaking term. The standard way to accomplish bulk-breaking is to add a scalar bulk field, and to let it obtain a vacuum expectation value. However, the KK decomposition of the bulk scalar would introduce 4D scalar resonances, which we want to avoid for simplicity in the present paper. Rather, in the HTC Lagrangian (9), we introduced a position dependent kinetic term mixing L and R gauge fields, which is invariant under the vector gauge symmetry and parity. Obviously, many more terms besides $F_L F_R$ could be added to the Lagrangian and may lead to different phenomenology, but $F_L F_R$ is the operator with lowest dimension and number of derivatives and no new fields.

From the effective field theory point of view, what matters is that bulk-breaking allows a more general spectrum and structure for the cubic interactions of (2), see Sec. VI C.

D. Dialing the effective warp factors

Our parameterization of the spin-1 sector is economical. Three combinations of parameters are set by imposing the physical value of M_W, M_Z, $\alpha_{\rm em}$. The remaining parameters can be chosen as the size l_1 of the extra dimension (closely related to the mass of the lightest resonance, M_{W_1}) and the two parameters o_V and o_A describing the functional shape of the effective background felt by the spin-1 fields.

For the fermion sector, we choose the couplings of the fermions to the W, Z, γ to follow the SM relations. As to the couplings of fermions to resonances, they do not influence the results of this paper, as long as these are suppressed by a factor compared to the couplings to SM gauge fields.[2]

[1] A bulk $U(1)_{B-L}$ would introduce more neutral resonances, as in Higgsless models. In either case, an extra parameter enters the Lagrangian.

[2] In the phenomenological study [11], we set the couplings between any fermions and a resonance $W_{1,2}$ or $Z_{1,2}$ to be equal to the coupling between the same fermions and the W or Z, respectively, rescaled by a common factor κ, independent of the fermion or the resonance multiplet. For the specific points studied in [11] with 500 and 600 GeV resonances, we chose $\kappa = 1/20$ and $\kappa = 1/10$ in order for the resonances to have avoided detection at Tevatron [36–42].

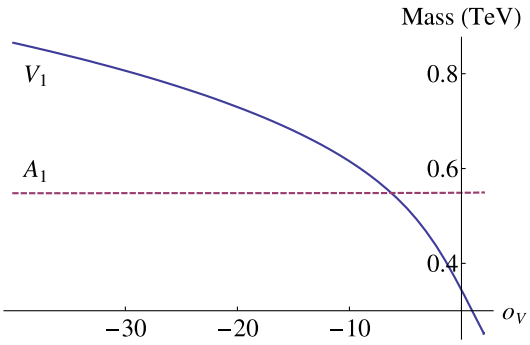

FIG. 1 (color online). Mass of the lightest vector (V_1) and lightest axial (A_1) resonances as a function of o_V, for $o_A = 0$, $l_1 = 7$ TeV^{-1}. This plot uses Dirichlet BCs in the UV.

Let us point out the basic effects of varying one of the parameters o_V. A negative o_V in the effective warp factor (17) acts as an IR cutoff, effectively shortening the space in which V fields live, but leaving axial masses untouched. Figure 1 shows this explicitly in a simpler scenario with UV Dirichlet BCs for V and A fields ($V = A = 0$ at the UV brane). With such BCs, the first axial resonance would be lighter than the vector one for $o_V < -5$. For applications to EWSB, the situation is more complicated due to the different BCs, see Sec. IV.

IV. PARITY OF RESONANCES

The HTC Lagrangian (9) is invariant under parity ($L \leftrightarrow R$). One would thus expect the spin-1 resonances to have definite parity. In the 5D language, the eigenfunctions would then split into two distinct sectors: V or A wave functions, not admixtures of them. However, the coupling to electroweak $\mathrm{SU}(2)_L \otimes \mathrm{U}(1)_Y$ interactions breaks parity. In the 5D language, this effect comes from the UV BCs which mix the vector and axial sectors (15).

The mixing effects depicted in Fig. 2 become especially important for nearly degenerate resonances, the region we want to look at. This mixing is not an artifact of our framework and will hold for any model of nearly degenerate resonances coupled to the electroweak sector. As can be seen in Fig. 2, the level repulsion also affects the higher KK modes.

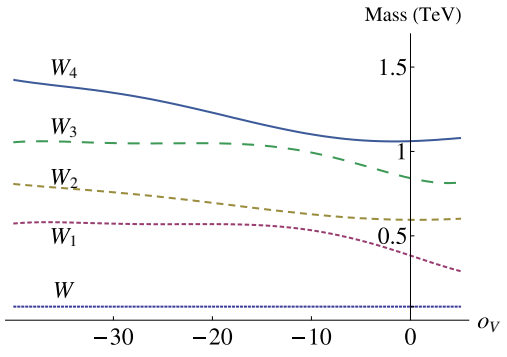

FIG. 2 (color online). Masses of the four lightest charged resonances in TeV, as a function of o_V, for $o_A = 0$, and fixing $l_1 = 7$ TeV^{-1} with M_W at its physical value.

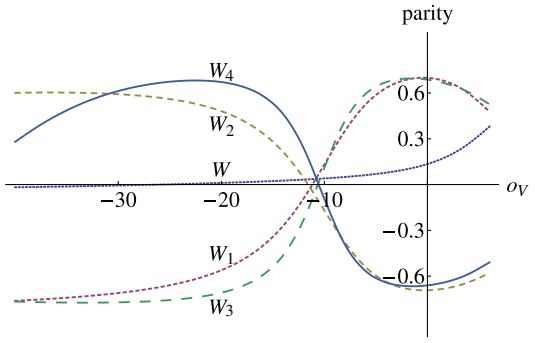

FIG. 3 (color online). Parity, as defined in (18), of the various charged modes as a function of o_V, for $o_A = 0$ and $M_{W_1} = 500$ GeV, and $l_1 = 7$ TeV^{-1}.

Because of the mixing, each eigenstate is a linear combination of a vector and an axial wave function, without definite parity. The eigenfunctions are thus two-component objects $|\Psi\rangle = |V_\Psi, A_\Psi\rangle$, where V_Ψ and A_Ψ are the vector and axial component. To follow what happens as we vary the effective warp factors, we define the continuous parity of eigenstate Ψ by

$$\text{parity}\,(\Psi) = \frac{\int dz (w_V V_\Psi^2 - w_A A_\Psi^2)}{\int dz (w_V V_\Psi^2 + w_A A_\Psi^2)}, \qquad (18)$$

and plot the parity of the states as we vary o_V in Fig. 3.

Figure 3 shows that the lightest resonance goes adiabatically from a mostly vector state for $o_V \approx 0$, to a mostly axial one for large negative o_V, and vice versa for the second level. Figure 3 also shows that the W, whose UV BC (15) imposes it to be predominantly $V - A$ in the UV, contains nearly equal admixtures of V and A for most of the parameter space. The resonances change parity near $o_V \simeq -10$.

The fact that V and A mix to yield mass eigenstates without definite parity will have important consequences later on in Sec. VI C for the scenarios we consider. On the other hand, the mixing is not relevant for Higgsless models, since it decreases with the mass separation between states.

V. BOUNDS FROM TGCS

In the present section, we examine the limits set by TGCs on resonance masses and point to regions in the remaining two-dimensional parameter space (o_V, o_A) where $M_{W_1} \leq 500$ GeV is allowed.

To avoid numerical difficulties encountered when studying the whole parameter space, we restrict ourselves to two curves within the (o_A, o_V) plane, along which we illustrate the constraints from TGCs in this section. Our choices are line A ($o_A = 0$) and line B ($\alpha_1 = 0$), where α_1 is the Longhitano coefficient of the $W^3_{\mu\nu} B^{\mu\nu}$ term. (See Appendix A for details).

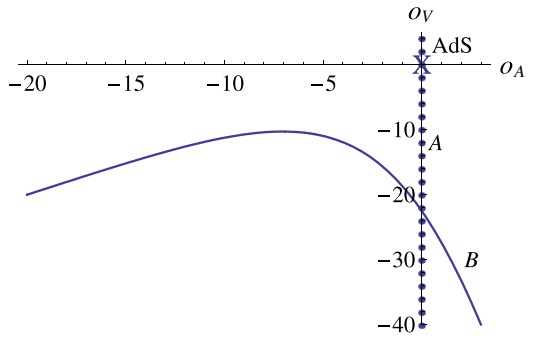

FIG. 4 (color online). The (o_A, o_V) plane, with lines A and B (dotted and continuous, respectively) studied in the text. The approximation $l_0 \to 0$ has been used to determine line B. The origin of the axes corresponds to the pure AdS Higgsless model.

The two curves (line A and line B) are depicted in the (o_A, o_V) space in Fig. 4, where the origin of the plot represents AdS space. The curve also shows how the physical predictions depend not only on the difference $o_A - o_V$, but on both effective warp factors.

Line B imposes a relation between o_A and o_V, and we will plot the various couplings as a function of o_A along that curve.

A. Line A: $o_A = 0$

The TGCs are the main constraint on HTC, since oblique corrections (S, T) vanish by our choice of fermion couplings to gauge fields. In Fig. 5, we depict the 2σ constraints on M_{W_1} imposed by the bounds on each of the TGCs. Figure 5 shows that resonances as light as 500 GeV are allowed by the TGC constraints, but only for $o_V \lesssim -10$. On the other hand, we see that a model in a pure AdS background ($o_A = o_V = 0$) is incompatible with the TGC bounds at 2σ unless M_{W_1} is raised above 700 GeV.

B. Line B: $\alpha_1 = 0$

We study the line for which the Longhitano coefficient α_1 vanishes. Our motivation for studying this line is twofold. First, a vanishing α_1 limits the deviations of the TGCs

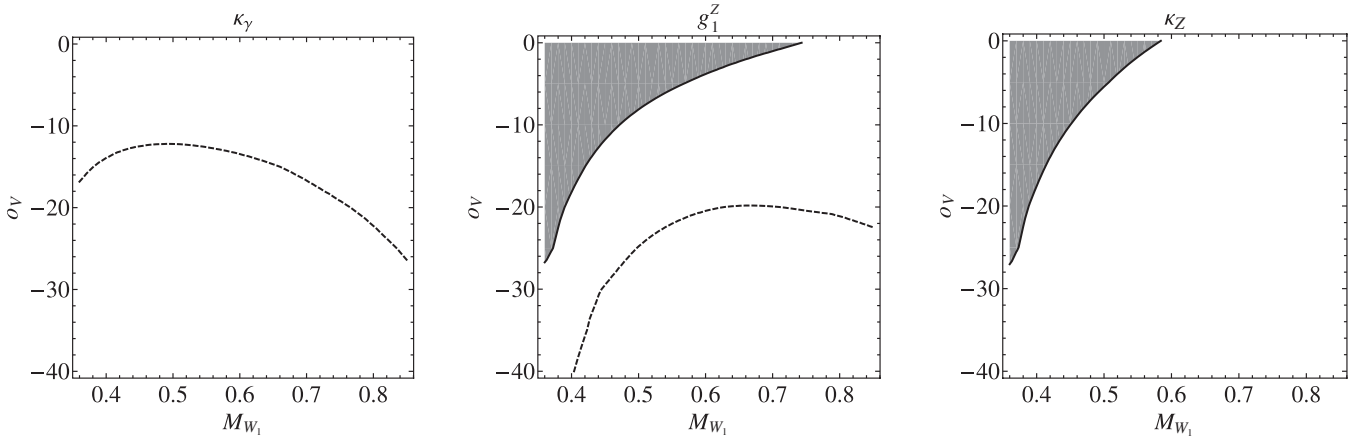

FIG. 5. 2σ bounds imposed by κ_γ, g_1^Z, κ_Z in the space of M_{W_1} (horizontal axis) and o_V (vertical axis), along line A ($o_A = 0$). Darker areas are excluded, and the central value is depicted as a dashed line.

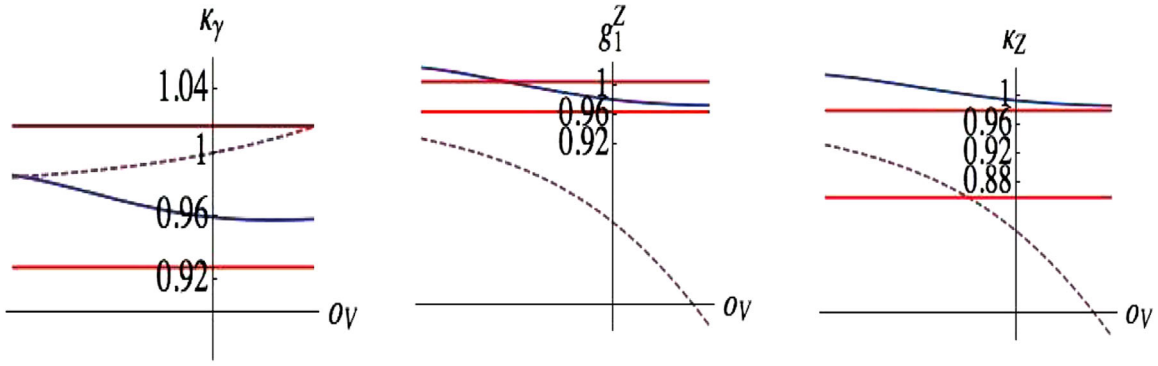

FIG. 6 (color online). TGCs along line B, for $M_{W_1} = 500$ GeV, with all other parameters at their physical value. The horizontal axis depicts the central value measured at LEP, while the solid horizontal bands depict the 1σ errors. The dashed line indicates the TGC values if the approximation $\ell_0 \to 0$ is made. The discrepancy between the actual and approximate TGCs is explained in more detail in Appendix A 1.

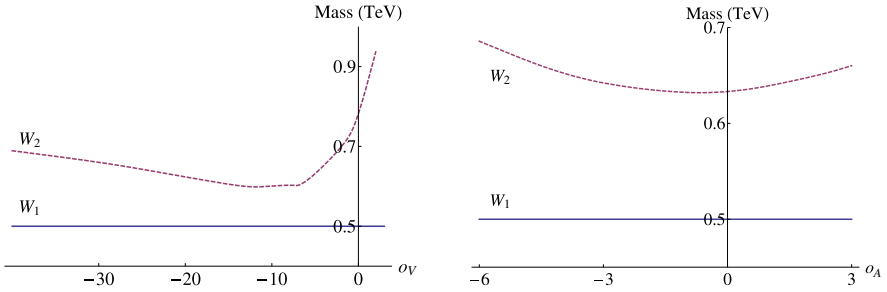

FIG. 7 (color online). Variation of M_{W_2} along the two curves in parameter space, when M_{W_1} is set to 500 GeV. Other parameters are set to reproduce the physical values of α, M_W, M_Z.

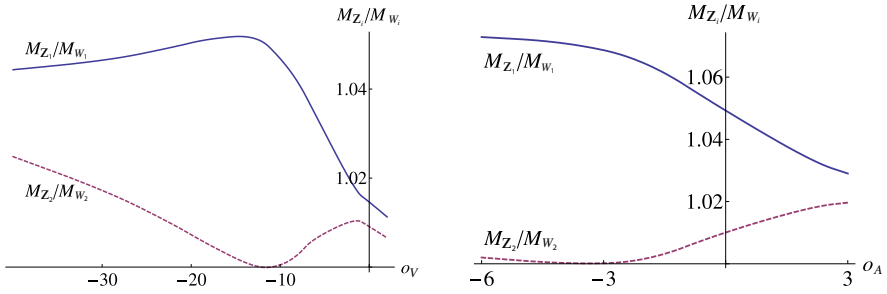

FIG. 8 (color online). Ratios of masses M_{Z_1}/M_{W_1} and M_{Z_2}/M_{W_2} along the two curves in parameter space, for $M_{W_1} = 500$ GeV. Other parameters are set in order to reproduce the physical values of α, M_W, M_Z.

from the SM, see (A6)–(A8) in Appendix A. This is illustrated in Fig. 6, where the TGCs are plotted along the line of $\alpha_1 = 0$, for $M_{W_1} = 500$ GeV. Additionally, since α_1 describes the mixing between W^3 and the hypercharge gauge field B, $\alpha_1 = 0$ means that no additional contributions are required to cancel the S parameter.

VI. SPECTRUM AND COUPLINGS

In this section, we set the mass of the lightest resonance to $M_{W_1} = 500$ GeV. We then extract predictions for resonance couplings along the two lines A and B described in Sec. V. This particular choice is arbitrary, but exemplifies the phenomenology that can be obtained in HTC.

In practice, we will truncate the KK tower, explicitly keeping in the Lagrangian only the first two multiplets of resonances: with the lightest resonance at 500 GeV, the third multiplet would usually come in above 1 TeV (see Fig. 2), still interesting for the LHC purposes but outside the scope of the present paper.

A. Spectrum

The splitting between multiplets determines the decays of the heavy resonance. A splitting larger than ~100 GeV allows for the W_2 to decay into W_1.

Figure 7 depicts the mass of W_2 when M_{W_1} is set to 500 GeV. The left plot for line A corresponds to the one of Fig. 2 above, but rather than keeping l_1 fixed, it is rescaled to maintain $M_{W_1} = 500$ GeV. Along this line (line A), the splitting between resonances decreases from the AdS ($o_V = o_A = 0$) as we dial a nonzero value of o_V. Along line B ($\alpha_1 = 0$), the separation between the two lightest resonances remains about 150 GeV. As the overall scale for resonance mass increases, the splitting decreases.

Along the same two lines, we can examine the isospin splitting within the lightest two triplets of resonances, as plotted in Fig. 8. This mass splitting affects the ρ parameter, which will remain close to unity as long as the couplings of fermions to resonances are small enough.[3] The neutral resonances are always heavier than the charged ones, due to the UV BC (15), which lifted the Z with respect to the W.

B. Coupling of resonances to WW: new contributions

In this section, we discuss how a selection rule that was valid in previous models does not apply to HTC. In the limit where the SM gauge couplings vanish, the system recovers a $L \leftrightarrow R$ symmetry under which all resonances are either even or odd under parity. In this parity-limit, only the vector resonances would couple to two W's

[3]We do not compute ρ here, as it depends on the value of these couplings (in particular, it depends on κ in the example mentioned in footnote [2]). Since we have already assigned SM couplings between the fermions and the W, Z, the T parameter vanishes.

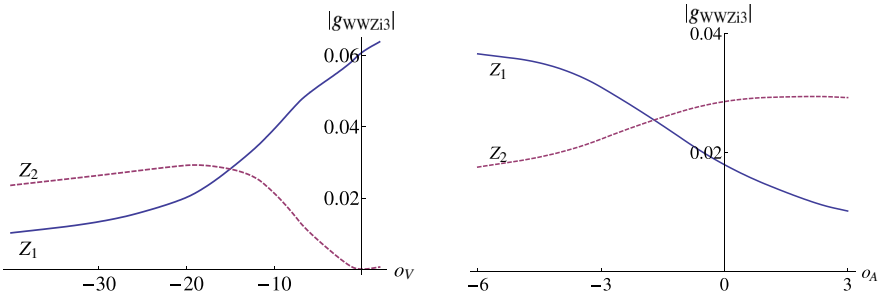

FIG. 9 (color online). Coupling g_{WWZ_i3} of the two lightest neutral resonances Z_1, Z_2 to two $W's$, along the two usual curves in parameter space. Other parameters are set in order to produce $M_{W_1} = 500$ GeV, as well as the physical values of α, M_W, M_Z.

$$g_{VW_LW_L} \neq 0, \qquad g_{AW_LW_L} = 0, \tag{19}$$

and thus only the vector resonances help unitarize W_LW_L scattering.

As seen in Sec. IV, once the SM gauge interactions are turned on, the LR parity is violated: the axial or vector labels become meaningless as both towers of resonances acquire both components. Given that all resonances have a vector component, they all couple to the W and Z. This means that both sets of resonances participate in unitarizing longitudinal gauge boson scattering.

Figure 9 shows, along the two usual lines in parameter space, the coefficient g_{WWZ_i3} in the term

$$-ig_{WWZ_i3}\partial_{[\mu}Z^i_{\nu]}W^{-\mu}W^{+\nu}. \tag{20}$$

Since both light resonances have cubic couplings with two SM gauge fields, they can both be searched for in WZ final states [11]. In the case of AdS, we recover that the vector resonances couple predominantly to WW, while the axial ones nearly decouple. Making o_V negative partially reverses the situation, as expected from Figs. 1 and 3: the second lightest resonance is now more coupled to WW than the first one is.

C. New cubic couplings

In the present section, we detail how different effective warp factors affect the cubic couplings. In particular, it turns out that $o_A \neq o_V$ allows for new couplings with interesting phenomenological consequences.

When the two effective warp factors are equal, the TGCs (1) satisfy

$$\kappa_\gamma = 1, \tag{21}$$

$$\kappa_Z = g_1^Z. \tag{22}$$

More generally, equality of the two effective warp factors implies that, for any three spin-1 particles B, C, D the three couplings g_{BCD1}, g_{BCD2}, g_{BCD3} are equal, according to

$$\begin{aligned} g_{BCD1} &= g_{BCD2} = g_{BCD3} \\ &= -\frac{1}{\sqrt{2}}\int \frac{dz}{g_5^2} w(V_BV_CV_D + V_BA_CA_D + A_BV_CA_D \\ &\quad + A_BA_CV_D), \end{aligned} \tag{23}$$

where we have already used $w \equiv w_V = w_A$. Applied to photon couplings, this implies that the photon cannot mediate a transition between two different particles.

Deviating from a standard 5D AdS setup allows for a richer structure. In HTC, plugging in $V_X(A_X)$ for the vector (axial) component profile of field $X \subset \{W^\pm, Z, \gamma, W^\pm_{1,2}, Z_{1,2}\}$, we find

$$\begin{aligned} g_{BCD1} &= -\frac{1}{\sqrt{2}}\int \frac{dz}{g_5^2}(w_V(V_BV_CV_D + V_BA_CA_D) \\ &\quad + w_A(A_BV_CA_D + A_BA_CV_D)), \end{aligned} \tag{24}$$

$$\begin{aligned} g_{BCD2} &= -\frac{1}{\sqrt{2}}\int \frac{dz}{g_5^2}(w_V(V_CV_DV_B + V_CA_DA_B) \\ &\quad + w_A(A_CV_DA_B + A_CA_DV_B)), \end{aligned} \tag{25}$$

$$\begin{aligned} g_{BCD3} &= -\frac{1}{\sqrt{2}}\int \frac{dz}{g_5^2}(w_V(V_DV_BV_C + V_DA_BA_C) \\ &\quad + w_A(A_DV_BA_C + A_DA_BV_C)), \end{aligned} \tag{26}$$

where B, C are charged fields, and D is neutral. In the most general scenario, where the vector and axial warp factors are different and $B \neq C^*$, $D \neq \gamma$, the couplings of the three permutations can all be different

$$g_{BCD1} \neq g_{BCD2} \neq g_{BCD3}. \tag{27}$$

When B and C are antiparticles of each other, B and C share the same profile, so the two couplings with the derivative acting on a charged field are equal

$$g_{BBD1} = g_{BBD2} \neq g_{BBD3}. \tag{28}$$

When the neutral field is the photon, there is an additional constraint on the triboson couplings from $U(1)_{em}$ gauge invariance

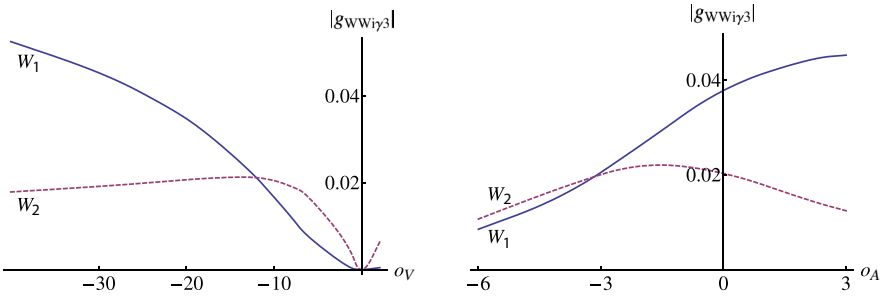

FIG. 10 (color online). Couplings $g_{WW_i\gamma 3}$ of the two lightest charged resonances W_1, W_2 to $W\gamma$ along the two usual curves in parameter space. Other parameters are set to produce $M_{W_1} = 500$ GeV, as well as the physical values of α, M_W, M_Z.

$$g_{BC\gamma 1} = g_{BC\gamma 2} = 0 \quad \text{for } B \neq C^*. \tag{29}$$

This result derives from the γ wave function being flat: the cubic overlap integrals (24) and (25) then reduce to a quadratic overlap corresponding to the orthogonality relations

$$\int dz(w_V V_\Psi V_\Phi + w_A A_\Psi A_\Phi) = 0, \quad \text{for } \Psi \neq \Phi. \tag{30}$$

On the other hand, the third photon coupling [i.e. (26) with $D = \gamma$] does not reduce to such an orthogonality relation: it would be written as (30), but with the warp factors swapped $w_V \leftrightarrow w_A$. Therefore, couplings such as $W^+W_1^-\gamma$ vanish in Higgsless models, but not in HTC. The new coupling is shown in Fig. 10 along the usual lines.

We see two effects at play: first, unequal warp factors $o_A \neq o_V$ allow for a coupling of the axial resonance to $W\gamma$, and second, the mixing also allows a coupling of the vector resonance to $W\gamma$. Hence both resonances can decay to $W\gamma$, as studied in [11].

VII. CONCLUSION

We take a pragmatic approach to the description of dynamical electroweak symmetry breaking, providing a resonance Lagrangian simple enough to be implemented in Monte Carlo simulations, yet complex enough to incorporate phenomena beyond those usually considered. Our description of new strong interactions does not rely on an explicit model, but rather introduces phenomenological parameters describing the interactions of new states visible at the LHC.

Such an effective description usually comes at a price, namely, the large number of unknown parameters to be varied. We deal with this problem by imposing relations between the constants appearing in the effective Lagrangian: we construct our effective Lagrangian using rules from extra-dimensional model building in order to impose constraints (we could equally well have retained a fully 4D formulation by relying on mooses). On the other hand, we also want to lift some of the 5D constraints that seem too restrictive. To avoid the alternating spectrum and selection rules usually predicted by the usual 5D or moose approach, we work with an extension of the 5D framework: Holographic Technicolor (HTC), which starts as a 5D model, but adds as a new ingredient an effective bulk-breaking term without introducing new states other than spin-1 resonances.

We do not try to reproduce specific models in the literature, but instead study the phenomenology of new scenarios that evade some of the usual constraints on technicolor models. The UV completions of such scenarios are unknown, but we assume in our effective description that the problem of oblique corrections is solved, and set the couplings of fermions to W, Z accordingly. We also choose the couplings of SM fermions to resonances to pass experimental bounds.

We rely on bounds from the trilinear gauge couplings to restrict our three free parameters, and find that low-mass resonances (≤ 500 GeV) are allowed. Working in this low-mass assumption, we consider two interesting curves in the remaining two-parameter space. Two new couplings that our Lagrangian generally includes turn out to be relevant in these regions, allowing both light resonances to be seen in the WZ channel (as well as in the WW channel), and to decay to $W\gamma$ (observable at LHC).

Regarding future developments, we point out that our choice of effective description (drawing on the 5D formalism) allows for an easy inclusion of additional fields, such as scalars, technipions, or the isospin-singlet technicomega.

ACKNOWLEDGMENTS

We thank T. Appelquist, R. S. Chivukula, and W. Skiba for helpful comments. J. H. and A. M. are supported by DOE Grant No. DE-FG02-92ER-40704; V. S. is supported by DE-FG02-91ER40676. J. H. and V. S. acknowledge the hospitality of the Kavli Institute for Theoretical Physics in Santa Barbara, CA, where part of this work was completed.

APPENDIX A: TGCS

In this appendix, we detail a subtlety in the derivation of TGCs in our framework as compared to other approaches.

1. Electroweak chiral Lagrangian

The electroweak chiral Lagrangian [45] describes the electroweak sector without the Higgs boson at low energies. It is constructed by coupling the Yang-Mills action of $SU(2)_L \otimes U(1)_Y$

$$\mathcal{L}_{\rm YM} = -\tfrac{1}{4}F^a_{\mu\nu}F^{a,\mu\nu} - \tfrac{1}{4}B_{\mu\nu}B^{\mu\nu}, \tag{A1}$$

to a chiral Lagrangian for the three Goldstone bosons (GBs) of the breaking $SU(2) \times SU(2) \to SU(2)$—this is the minimal custodial sector that feeds 3 GBs without introducing technipions. This GB chiral Lagrangian, ordered by the number of derivatives, starts with the operator[4]

$$\mathcal{L}_{D^2} = \frac{f^2}{4}\langle D_\mu U^\dagger D^\mu U\rangle, \tag{A2}$$

where $\langle\ \rangle$ means SU(2) trace and the covariant derivative applied to the GB unitary matrix U reads

$$D_\mu U = \partial_\mu U - igW_\mu U + ig'B_\mu U\frac{\tau^3}{2}. \tag{A3}$$

The covariant derivative couples the weak $SU(2)_L \otimes U(1)_Y$ gauge fields to the GBs. This can be checked by going to unitary gauge, i.e. $U = \mathbb{1}$, which yields the appropriate masses for the $W^\pm$ and Z^0.

At the next order in the derivative expansion, there are extra quadratic (α_1), cubic (α_2, α_3), and quartic (α_4, α_5) couplings among the γ, W, Z

$$\begin{aligned}\mathcal{L}_{D^4} = {}& \alpha_1 g g' B_{\mu\nu}\left\langle U\frac{\tau^3}{2}U^\dagger W^{\mu\nu}\right\rangle \\ & + i\left\langle\left(\alpha_2 g W_{\mu\nu} + \alpha_3 g' B_{\mu\nu}\frac{\tau^3}{2}\right)[UD^\mu U^\dagger, UD^\nu U^\dagger]\right\rangle \\ & + \alpha_4\langle D_\mu U D_\nu U^\dagger\rangle^2 + \alpha_5\langle D_\mu U D^\mu U^\dagger\rangle^2.\end{aligned} \tag{A4}$$

Assuming that the underlying strong dynamics respect parity symmetry results in $\alpha_2 = \alpha_3$.[5]

The α_1 term introduces the mixing of W^3_μ and B_μ, even though the quadratic Lagrangian may have been diagonalized at the previous order; α_1 is thus an oblique correction. One may choose to diagonalize the full quadratic Lagrangian at this order (i.e. including α_1) in order to work in the mass basis, thereby shifting the deviation from the SM into fermion couplings [46].

[4]In the present framework, T vanishes; therefore, we do not write the corresponding operator.

[5]The Longhitano couplings α_i are related to the Gasser-Leutwyler L_i couplings (which assume parity invariance) by $\alpha_1 = L_{10}$, $\alpha_2 = \alpha_3 = -L_9/2$. The α_i coefficients with $i > 5$ introduce isospin breaking at tree level, and will therefore not be generated in our framework.

In the framework of HTC, α_1 is computed as follows:

$$\alpha_1 = -\frac{1}{2}\int_{l_0}^{l_1}\frac{dz}{g_5^5}\left(w_V(z) - w_A(z)\left(\frac{\int_z^{l_1} dz'/w_A(z')}{\int_{l_0}^{l_1} dz''/w_A(z'')}\right)^2\right), \tag{A5}$$

which is the expression used to determine the shape of line B in Fig. 4.

The cubic terms in α_1 as well as α_2, α_3 in the Lagrangian (A4) produce deviations from the SM in the TGCs (1), given by [47] (assuming $\alpha_2 = \alpha_3$)

$$\kappa_\gamma - 1 = \frac{e^2}{s^2}(-\alpha_1 + 2\alpha_3), \tag{A6}$$

$$g_1^Z - 1 = \frac{e^2}{c^2}\left(\frac{\alpha_1}{c^2 - s^2} + \frac{\alpha_3}{s^2}\right), \tag{A7}$$

$$\kappa_Z - 1 = e^2\left(\frac{2\alpha_1}{c^2 - s^2} + \frac{c^2 - s^2}{c^2 s^2}\alpha_3\right). \tag{A8}$$

This derivation uses the standard relation

$$G_F = \frac{g^2}{4\sqrt{2}M_W^2} = \frac{1}{\sqrt{2}f^2}, \tag{A9}$$

which is valid for the electroweak chiral Lagrangian, but not true in general. Indeed, relation (A9) assumes that g appearing in the covariant derivative (A3) is strictly equal to the fermion-W coupling, something which does not hold in our framework, nor in standard 5D models [43].

2. TGCs in Holographic Technicolor

We chose to *define* the interactions of the fermions by assigning them couplings to the physical mass eigenstates that satisfy the SM relations. Therefore, the S and T parameters will vanish. On the other hand, we model the interactions of spin-1 fields, imposing experimental values for the parameters α, M_Z, M_W, and predicting the TGCs. As a consequence, relations between fermion couplings (which are set by hand) and quantities involving γ, W, Z (which are predicted from a 5D Lagrangian) are modified. For example,

$$M_W \neq \frac{gf}{2} \tag{A10}$$

does not hold at tree level if g means the fermion-W coupling—this coupling is set by hand outside any 5D modelling, whereas M_W and f are an output of the 5D model. In other words, we have in general

$$f \neq 246\ \text{GeV}. \tag{A11}$$

As a consequence, we find that, while relation (A6) holds in our framework, the same is not true of (A7) and (A8). This is because these latter two definitions depend on the value of the Weinberg angle, defined as

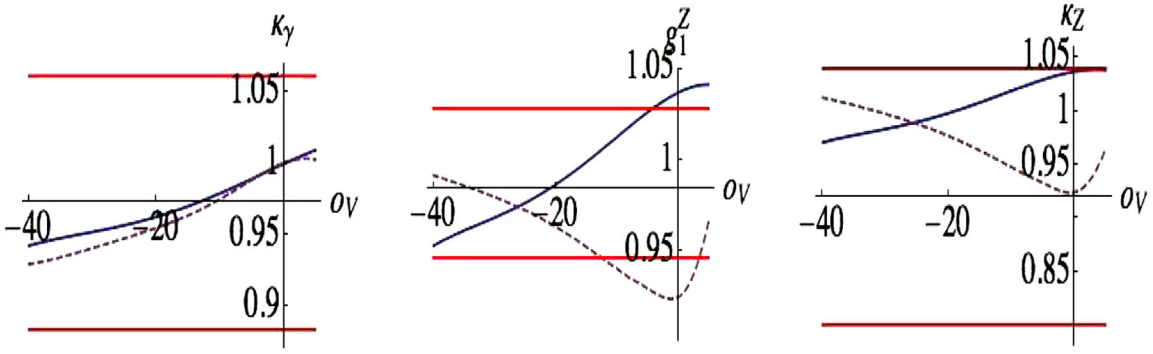

FIG. 11 (color online). TGCs along line A, for $M_{W_1} = 500$ GeV, with all other parameters at their physical value. The horizontal axis depicts the central value measured at LEP, while the solid bands depict the 1σ errors. The continuous lines depict the TGCs as a function of o_V, for $o_A = 0$ and $M_{W_1} = 500$ GeV. Dashed lines represent values computed from blindly using (A6) and (A7). The discrepancy in the κ_γ plot comes from having used the $l_0 \to 0$ approximation for the dashed line.

$$s^2 c^2 = \frac{\pi\alpha}{\sqrt{2} G_F M_Z^2}. \tag{A12}$$

The extraction of the TGCs thus involves G_F and not f whereas Eqs. (A6)–(A8) assumed a relation between the two, Eq. (A9). The definition of the Weinberg angle (A12) feeds into the extraction of the TGCs from the Lagrangian (1). Figure 11 compares the exact prediction of the TGCs with the one that would be derived from (A6)–(A8).

To understand the discrepancy, we must go back to the definitions of G_F

$$G_F = \frac{1}{4\sqrt{2}} \left(\frac{g^2}{M_W^2} + \sum_{n=1} \frac{g_n^2}{M_{W_n}^2} \right), \tag{A13}$$

where g, g_n are the fermion-spin-1 couplings, and f [48]

$$\frac{1}{f^2} = 2 \sum_{n=0} \frac{A_{W_n}(l_0)^2}{M_{W_n}^2}. \tag{14}$$

There is no connection between f and G_F unless the fermions are modeled in 5D in a particular way. If, for example, the fermions were placed on the UV brane, then there would be a relation between the g_n's of (A13) and the wave functions $A_n(l_0)$ of the resonances on the UV brane.

[1] Steven Weinberg, Phys. Rev. D **19**, 1277 (1979).
[2] Leonard Susskind, Phys. Rev. D **20**, 2619 (1979).
[3] Edward Farhi and Leonard Susskind, Phys. Rep. **74**, 277 (1981).
[4] Nima Arkani-Hamed, Massimo Porrati, and Lisa Randall, J. High Energy Phys. 08 (2001) 017.
[5] R. Rattazzi and A. Zaffaroni, J. High Energy Phys. 04 (2001) 021.
[6] Nima Arkani-Hamed, Andrew G. Cohen, and Howard Georgi, Phys. Rev. Lett. **86**, 4757 (2001).
[7] Hsin-Chia Cheng, Christopher T. Hill, Stefan Pokorski, and Jing Wang, Phys. Rev. D **64**, 065007 (2001).
[8] Andreas Birkedal, Konstantin T. Matchev, and Maxim Perelstein, Phenomenology of Higgsless Models at the LHC and the ILC, 2005.
[9] Hong-Jian He *et al.*, LHC Signatures of New Gauge Bosons in Minimal Higgsless Model, 2007.
[10] Georges Azuelos *et al.*, Low-Scale Technicolor at the LHC, 2008, in Brooijmans [49].
[11] J. Hirn, A. Martin, and V. Sanz, J. High Energy Phys. 05 (2008) 084.
[12] M. Bando, T. Kugo, S. Uehara, K. Yamawaki, and T. Yanagida, Phys. Rev. Lett. **54**, 1215 (1985).
[13] R. Casalbuoni, S. De Curtis, D. Dominici, and R. Gatto, Nucl. Phys. **B282**, 235 (1987).
[14] Masako Bando, Taichiro Kugo, and Koichi Yamawaki, Phys. Rep. **164**, 217 (1988).
[15] R. Casalbuoni, S. De Curtis, D. Dominici, F. Feruglio, and R. Gatto, Int. J. Mod. Phys. A **4**, 1065 (1989).
[16] Roshan Foadi, Shrihari Gopalakrishna, and Carl Schmidt, J. High Energy Phys. 03 (2004) 042.
[17] J. Hirn and J. Stern, Eur. Phys. J. C **34**, 447 (2004); R. Foadi, M. T. Frandsen, T. A. Ryttov, and F. Sannino, Phys. Rev. D **76**, 055005 (2007); D. D. Dietrich and C. Kouvaris, Phys. Rev. D **78**, 055005 (2008).
[18] Roberto Contino, Yasunori Nomura, and Alex Pomarol, Nucl. Phys. **B671**, 148 (2003).
[19] Gustavo Burdman and Yasunori Nomura, Phys. Rev. D **69**, 115013 (2004).
[20] Juan Martin Maldacena, Adv. Theor. Math. Phys. **2**, 231 (1998); Int. J. Theor. Phys. **38**, 1113 (1999).
[21] S. S. Gubser, Igor R. Klebanov, and Alexander M.

Polyakov, Phys. Lett. B **428**, 105 (1998).
[22] Edward Witten, Adv. Theor. Math. Phys. **2**, 253 (1998).
[23] D. T. Son and M. A. Stephanov, Phys. Rev. D **69**, 065020 (2004).
[24] Joshua Erlich, Emanuel Katz, Dam T. Son, and Mikhail A. Stephanov, Phys. Rev. Lett. **95**, 261602 (2005).
[25] Leandro Da Rold and Alex Pomarol, Nucl. Phys. **B721**, 79 (2005).
[26] J. Hirn and V. Sanz, J. High Energy Phys. 12 (2005) 030.
[27] J. Hirn, N. Rius, and V. Sanz, Phys. Rev. D **73**, 085005 (2006).
[28] Johannes Hirn and Veronica Sanz, Phys. Rev. Lett. **97**, 121803 (2006).
[29] Michael Edward Peskin and Tatsu Takeuchi, Phys. Rev. D **46**, 381 (1992).
[30] Csaba Csaki, Christophe Grojean, Luigi Pilo, and John Terning, Phys. Rev. Lett. **92**, 101802 (2004).
[31] Kaustubh Agashe, Csaba Csaki, Christophe Grojean, and Matthew Reece, J. High Energy Phys. 12 (2007) 003.
[32] R. Sekhar Chivukula and Elizabeth H. Simmons (private communication).
[33] K. Hagiwara, R. D. Peccei, D. Zeppenfeld, and K. Hikasa, Nucl. Phys. **B282**, 253 (1987).
[34] J. Hirn, A. Martin, and V. Sanz, Technivectors at the LHC, in Brooijmans [49].
[35] R. S. Chivukula, E. H. Simmons, H. J. He, M. Kurachi, and M. Tanabashi, Phys. Rev. D **70**, 075008 (2004).
[36] King-man Cheung, Phys. Lett. B **517**, 167 (2001).
[37] V. M. Abazov *et al.*, Phys. Rev. D **71**, 091108 (2005).
[38] A. Abulencia *et al.*, Phys. Rev. D **75**, 091101 (2007).
[39] A. Abulencia *et al.*, Phys. Rev. Lett. **98**, 161801 (2007).
[40] T. Aaltonen *et al.*, Phys. Rev. Lett. **99**, 171802 (2007).
[41] CDF Collaboration, CDF Note 8452, 2007, http//www-cdf.fnal.gov/physics/exotics/r2a/20060817.heavy_obj_wz_paramonov/highPt_Z.html.
[42] CDF Collaboration, CDF Note 9150, 2007, http//www-cdf.fnal.gov/physics/new/top/2007/singletop/Wprime/Public_2fb.html.
[43] Csaba Csaki, Jay Hubisz, and Patrick Meade, Electroweak Symmetry Breaking from Extra Dimensions, 2005.
[44] Csaba Csaki, Christophe Grojean, Hitoshi Murayama, Luigi Pilo, and John Terning, Phys. Rev. D **69**, 055006 (2004).
[45] Anthony C. Longhitano, Nucl. Phys. **B188**, 118 (1981).
[46] Andreas Nyffeler and Andreas Schenk, Phys. Rev. D **62**, 113006 (2000).
[47] Bob Holdom, Phys. Lett. B **258**, 156 (1991).
[48] Johannes Hirn and Veronica Sanz, Phys. Rev. D **76**, 044022 (2007).
[49] G. Brooijmans *et al.* (New Physics Working Group), arXiv:0802.3715.